



## OPEN Correlation between imaging features of pure ground-glass opacities and pathological subtypes of lung minimally invasive adenocarcinoma and precursor lesions

Yanqiu Zhu<sup>1</sup>, Cui Yan<sup>2</sup>, Wenjie Tang<sup>1</sup>, Yani Duan<sup>1</sup>, Xiuzhen Chen<sup>1</sup>, Yunxu Dong<sup>1</sup>, Yuefei Guo<sup>1</sup>, Weimin Liu<sup>1</sup> & Jie Qin<sup>1</sup>✉

This study aimed to investigate the relationship between imaging features of pure ground-glass opacities (pGGOs) and the pathological subtypes of minimally invasive adenocarcinoma (MIA) and precursor lesions. A retrospective analysis was conducted on data from 1521 patients diagnosed with GGOs as lung adenocarcinoma or precursor lesions between January 2015 and March 2021. The pGGOs were categorized into atypical adenomatous hyperplasia (AAH) / adenocarcinoma in situ (AIS) and MIA groups. Clinical information and CT imaging features were collected. Statistical analysis, logistic regression, and receiver operating characteristic (ROC) curve analysis were performed. A total of 127 patients with 139 pGGOs were included. Maximum radiodensity, minimum radiodensity, mean radiodensity, variance, and skewness showed significant differences between the two groups. Maximum radiodensity and maximum cross-sectional area were identified as risk factors for pathology. The logistic regression model yielded an area under the curve (AUC) of 0.747 (95% CI, 0.666–0.816) for predicting pathological subtypes. The intensity features of pGGOs were found to be significantly different between AAH/AIS and MIA groups. Maximum radiodensity and skewness were independent risk factors for pathology. However, these features did not exhibit satisfactory diagnostic efficiency.

**Keywords** Pure ground-glass opacity, Lung adenocarcinoma, Tomography, X-Ray computed, Pathology

Lung cancer is a global health concern, ranking as the second most commonly diagnosed cancer and the leading cause of cancer-related deaths in 2020<sup>1–4</sup>. Among the histological subtypes of lung cancer, lung adenocarcinoma is the most prevalent<sup>5,6</sup>. Over the years, advancements in research have led to the identification of distinct pathological subtypes of lung adenocarcinoma, including atypical adenomatous hyperplasia (AAH), adenocarcinoma in situ (AIS), minimally invasive adenocarcinoma (MIA), and invasive adenocarcinoma (IAC)<sup>7,8</sup>. Recently, AAH and AIS have been recognized as precursor lesions to lung adenocarcinoma<sup>9</sup>.

Studies have demonstrated that patients with precursor lesions and MIA have a favorable prognosis, with a 5-year disease-free survival rate of up to 100% following surgery<sup>10–15</sup>. However, it has been observed that the invasive pattern of MIA can impact its prognosis. MIA with poorly differentiated invasive patterns, such as micropapillary or solid predominant patterns, is associated with a higher risk of recurrence or the development of metachronous adenocarcinoma, necessitating closer monitoring and additional treatment post-surgery<sup>16</sup>. The progression from AIS to MIA signifies a significant increase in disease severity. Therefore, accurate prediction of the pathological subtypes of lung adenocarcinoma holds great clinical significance for treatment decisions and prognosis.

<sup>1</sup>Department of Radiology, The Third Affiliated Hospital of Sun Yat-sen University, No. 600 Tianhe Road, Tianhe District, Guangzhou 510630, China. <sup>2</sup>Division of Cardiology, The First Affiliated Hospital of Guangzhou University of Chinese Medicine, No. 261 Longxi Road, Liwan District, Guangzhou 510130, China. ✉email: qinjie@mail.sysu.edu.cn

On computed tomography (CT) images, early-stage lung adenocarcinomas often manifest as ground glass opacities (GGOs)<sup>17–20</sup>. GGOs are characterized by hazy increased lung opacity while preserving the bronchial and vascular margins<sup>21</sup>. Based on density, GGOs can be further classified as pure ground glass opacity (pGGO) or mixed ground glass opacity (mGGO)<sup>22</sup>. Numerous studies have explored the diagnostic criteria and performance of CT imaging features in identifying the pathological subtypes of lung adenocarcinoma<sup>23–25</sup>. Most studies found that the appearance of invasive component mainly results in the solid component in CT imaging. However, most studies have included the IAC group where the area of invasive components is generally large enough to causes many visible features in CT imaging. Compared with IAC, the area of invasive component in MIA is rather small, which could only results in subtle changes in imaging that are difficult to be observed, especially in pGGO. Therefore, most of the CT features that could help pathological diagnosis were attributed to IAC instead of MIA. The difference between MIA and precursor lesions in CT imaging is still left to be less known. So, in our study, we focus on MIA and precursor lesions that appeared as pGGOs. Our study aimed to compare the semantic features we observed and the shape features and first-order features obtained from artificial intelligence among MIA and precursor lesion, which could help reveal the differences in CT imaging between the two subtypes. And we hope to determine the diagnostic value of these imaging features, which could offer new understanding of distinguishing MIA from precursor lesions. The imaging finding might be a great help in improving precise treatment of MIA and precursor lesions.

## Methods

### Research subjects

We retrospectively reviewed the clinical, pathological, and imaging data of 1521 patients who were diagnosed with lung adenocarcinoma or precursor lesions at our hospital between January 1, 2015, and March 1, 2021. These cases were selected based on specific inclusion and exclusion criteria. This retrospective study was reviewed and approved by the Ethic Committees of the Third Affiliated Hospital of Sun Yat-Sen University and informed consent was waived. All experiments were performed in accordance with relevant guidelines and regulations.

Inclusion criteria:

1. Patients who underwent surgical resection for lesions and were pathologically diagnosed with atypical adenomatous hyperplasia (AAH), adenocarcinoma in situ (AIS), or minimally invasive adenocarcinoma (MIA).
2. Patients who had a CT scan of the lung within 1 month before surgery.
3. Patients who did not receive any anti-tumor therapy before surgery.
4. Patients whose lesions appeared as pure ground-glass opacities (pGGOs) on CT.
5. Patients with peripheral lesions.
6. Patients with complete clinical information available in the electronic medical record system.

Exclusion criteria:

1. Patients who only underwent nodules pathological biopsy or bronchial biopsy, or had an uncertain pathological diagnosis.
2. Patients with poor-quality CT imaging due to significant motion artifacts.
3. Patients whose CT images could not be analyzed by the artificial intelligence scientific research platform system.

A total of 127 patients were included in the study, among which 139 cases had pGGOs. Twelve patients had two pGGOs each, while the remaining patients had a single pGGO (Supplemental Table S1). The pGGOs were further divided into two groups: AAH/AIS group and MIA group (Fig. 1).

### Clinical data collection

Clinical information, including patient name, gender, age, main symptoms, hospitalization number, examination number, pathology number, pathological diagnosis description, pathology type, date of pathology report, interval between the last CT scan before surgery and surgery, invasion of pleura, lymph nodes or blood vessels, surgical method, and smoking history, was collected from the electronic medical record system. The pathological diagnosis of each lesion, made by one pathologist, was reviewed and confirmed by another senior pathologist.

### CT scan and imaging features acquisition

CT scans were performed using a 320-slice Aquilion ONE CT scanner (Toshiba Medical Systems, Tokyo, Japan) and an IQon Spectral scanner (Philips Healthcare, Best, the Netherlands). The patients were positioned supine with their arms raised and head advanced. All scans were performed at the end of inspiration while holding the breath. The CT protocol included the following parameters: 120 kV, automatic tube current modulation (180 mA–440 mA), iterative reconstruction technique, detector 160/40 mm, collimation 0.5/0.625 mm, pitch 1.5, matrix 512 × 512, and rotation time 0.5/0.27 s. The reconstructed axial layer thickness and layer distance were 1 mm. Images were reconstructed using adaptive iterative dose reduction (AIDR 3D, Toshiba Medical Systems) or hybrid iterative reconstruction (iDose4, Philips Healthcare).

The CT images were independently reviewed by two radiologists who were blinded to the pathological type. The results were confirmed by a senior radiologist. The lung window was set to a window level of -600 HU and a window width of 1,600 HU, while the mediastinal window was set to a window level of 40 HU and a window width of 300 HU. pGGOs are defined as hazy increased lung opacities while preserving the bronchial and vascular margins and show no identifiable solid attenuation on lung window or soft-tissue on mediastinal window. The following semantic features of pGGOs were evaluated: lobe location, shape (round

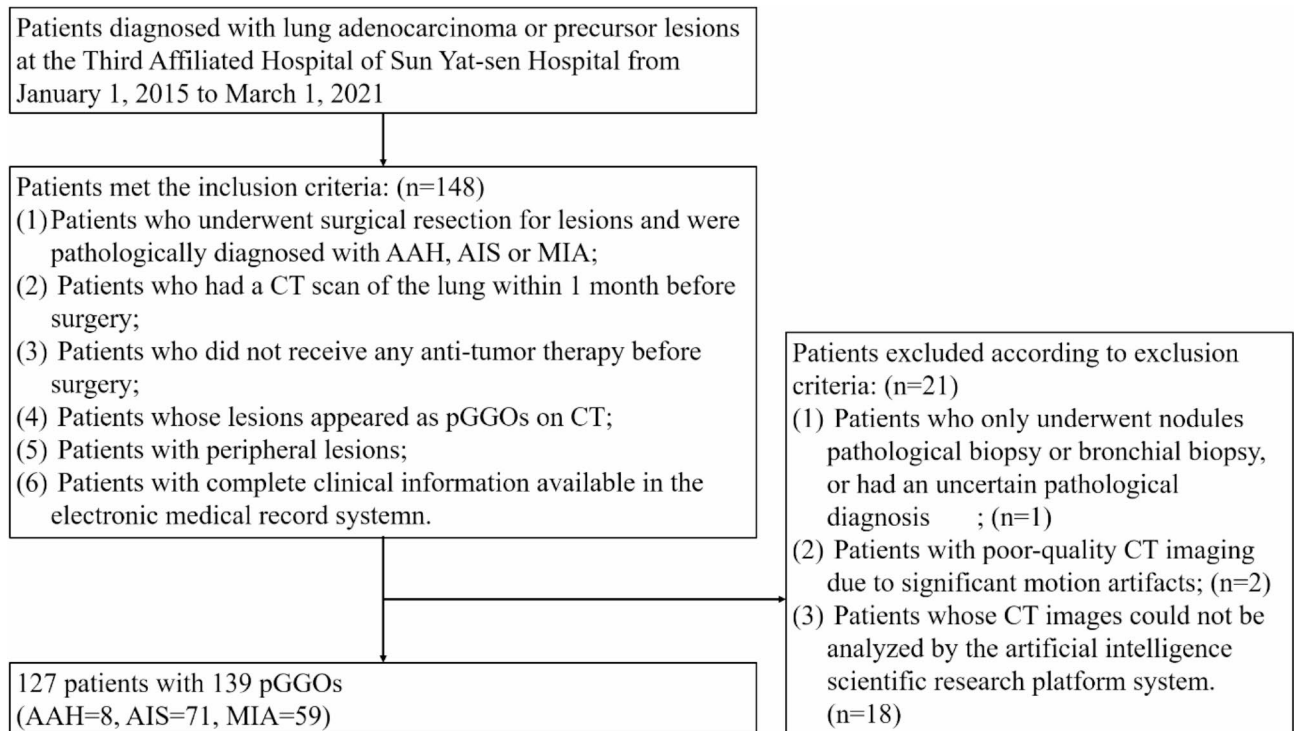


**Fig. 1.** Flow chart of inclusion.

or not), margin (clear or blurred), spiculation, lobulation, vacuole sign, air bronchogram, pleural indentation, vascular convergence sign, and pleural thickening. Spiculation was defined as a radial, unbranched, straight, fine, and short line that extended from the edge of the lung nodule. Lobulation was defined as a lobulated opacity formed by the arcuated and convex contour of the lung nodule. Vacuole sign was defined as a 1–2 mm punctate transparent shadow within the lung nodule. Air bronchogram was defined as the presence of air-filled (low-attenuated) bronchi in the background of low-air, high-attenuated pulmonary nodules. Pleural indentation was defined as the invagination, shrinkage, and shifting of the visceral pleura towards the lung nodules. Vascular convergence sign was defined as the appearance of one or more vessels drawn to or passing through the lesion or truncated at the edge of the lesion.

The CT images were uploaded to the Dr. Wise<sup>®</sup> artificial intelligence-assisted diagnosis system (Shenrui Medical, Beijing, China) to automatically segment the region of interest and extract shape features and first-order features, including maximum diameter, 3D maximum diameter, maximum cross-sectional area, volume, maximum radiodensity, minimum radiodensity, mean radiodensity, variance, kurtosis, skewness, surface area, compactness, sphericity, and entropy. Any discrepancies in the interpretation of CT images between the two radiologists were resolved through mutual consultation to obtain a final consistent result.

### Statistical analysis

Statistical analysis of the clinical data and CT imaging feature data was performed using IBM SPSS Statistics, version 25.0 (SPSS, Inc., Chicago, Ill., USA). The interobserver agreement on pGGOs was assessed by calculating Cohen's Kappa coefficients. The normality of quantitative data was evaluated using the Shapiro-Wilk test. Chi-square analysis, t-test, and Mann-Whitney U test were used to analyze the statistical differences in imaging features between the groups. Logistic regression was performed to compare the two groups and evaluate the risk of invasiveness. A forward elimination process was carried out in multivariate analysis. Receiver operating characteristic (ROC) analysis was used to evaluate the diagnostic accuracy of imaging features for different pathological subtypes. A p-value < 0.05 was considered statistically significant.

### Results

In this study, a total of 139 pGGOs were divided into two groups: AAH/AIS group (80 cases) and MIA group (59 cases). Reliability of interobserver agreement on pGGOs was good (Kappa = 0.934). Among the 127 patients included in the study, 34 were male (26.77%) and 93 were female (73.23%). The average interval between the last CT scan before surgery and surgery was  $11.20 \pm 7.34$  days. All AAH lesions and most AIS/MIA lesions were resected due to their adjacency to other resected invasive adenocarcinomas. Some AIS and MIA lesions were resected based on suspicious morphology (spiculation, lobulation, vacuole sign, etc.), persistent size  $\geq 10$  mm, or increase in size (Supplemental Table S2). There were no significant differences in clinical features between the two groups (Table 1).

Clinical characteristics	AAH / AIS (n = 64)	MIA (n = 51)	p	Cases
Gender			0.079	
Male	22 (34.38%)	10 (19.61%)		32 (27.83%)
Female	42 (65.62%)	41 (80.39%)		83 (72.17%)
Age	48.13 ± 11.46	49.39 ± 12.11	0.567	
Invasion			0.443	
Lymph node	0 (0%)	1 (1.96%)		1 (0.87%)
Surgery			0.644	
Nodule resection	35 (54.69%)	24 (47.06%)		59 (51.30%)
Wedge/segment resection	23 (35.94%)	20 (39.22%)		43 (37.39%)
Lobectomy	6 (9.38%)	7 (13.73%)		13 (11.30%)
Symptoms			0.239	
Absent	49 (76.56%)	34 (66.67%)		83 (72.17%)
Present	15 (23.44%)	17 (33.33%)		32 (27.83%)
Smoking history			0.460	
None	59 (92.19%)	49 (96.08%)		108 (93.91%)
Yes	5 (7.81%)	2 (3.92%)		7 (6.09%)

**Table 1.** Clinical characteristics of 115 patients diagnosed as MIA or precursor lesion with single pGGO. AAH, atypical adenomatous hyperplasia. AIS, adenocarcinoma in situ. MIA, minimally invasive adenocarcinoma. pGGO, pure ground-glass opacity.

Regarding CT imaging features, there was a statistically significant difference in spiculation between the two groups, while no differences were observed in the rest of the CT imaging signs (Table 2; Fig. 2). The maximum radiodensity, minimum radiodensity, mean radiodensity, variance, and skewness were found to be significantly different between the two groups. Specifically, pGGOs of AAH or AIS were more likely to show lower intensity, smaller variance, and larger skewness compared to MIA (Table 3). Univariate logistic regression analysis revealed that the levels of maximum radiodensity, minimum radiodensity, mean radiodensity, variance, skewness, and entropy were significantly associated with the pathological subtypes. Multivariate logistic regression analysis further identified maximum radiodensity and skewness as independent risk factors for MIA.

pGGOs with a maximum radiodensity of -430.00~-220.00 Hu and > -220.00 Hu had a 3.109-fold and 12.955-fold increased risk of MIA, respectively, compared to pGGOs with radiodensity < -430.00 Hu. Similarly, pGGOs with a skewness of -0.07~-0.02 had a 0.136-fold increased risk of MIA compared to pGGOs with skewness < -0.07 Hu (Table 4). The area under the curve (AUC) of the predicted value from the multivariate logistic regression was 0.747 (95% CI, 0.666-0.816), which was significantly larger than the AUC of maximum radiodensity (0.698 (95% CI, 0.614-0.773),  $p = 0.035$ ) and skewness (0.608 (95% CI, 0.522-0.690)). However, there was no significant difference between maximum radiodensity and skewness ( $p = 0.070$ ) (Fig. 3).

Discussion

In this study, we observed a higher proportion of female patients compared to male patients, which is consistent with previous studies<sup>12,26,27</sup>. This may be attributed to the increasing incidence of lung adenocarcinoma in women in recent years<sup>28</sup>. The age distribution of patients in our study is similar to previous studies, indicating a decreasing age of onset of lung cancer<sup>12,29</sup>.

The majority of patients in our study chose sublobectomy as it has a similar prognosis to lobectomy among the three pathological subtypes and allows for the preservation of more normal lung tissue with good function<sup>30,31</sup>.

The development from atypical adenomatous hyperplasia (AAH), adenocarcinoma in situ (AIS), and minimally invasive adenocarcinoma (MIA) to invasive adenocarcinoma (IAC) is a continuous evolution process<sup>8</sup>. In lesions with the pathological subtypes of AAH or AIS, tumor cells proliferate along the alveolar wall, leading to an increase in the thickness of the alveolar wall without collapse of the alveolar cavity. As tumor cells infiltrate and fibrotic components increase, an area of invasive adenocarcinoma measuring ≤ 5 mm in diameter appears, eventually developing into MIA<sup>32,33</sup>. These pathological changes can affect the texture, density, and morphology of the lesion.

Our study found that spiculation was more likely to appear in pGGOs of MIA compared to precursor lesions. This may be attributed to the direct infiltration of the tumor into adjacent bronchovascular sheaths in MIA. Previous studies have also highlighted the importance of morphology features of ground-glass opacities (GGOs) in predicting invasiveness<sup>34-36</sup>. However, in our study, most semantic features were not significantly different between precursor lesions and MIA. This may be because MIA lesions begin to appear with invasive components and increased tumor heterogeneity, resulting in subtle pathological changes that do not manifest visibly in morphology.

Our study also found that differences between precursor lesions and MIA were primarily attributed to intensity features, indicating that subtle progression in pathology may be manifested by intensity features to some extent. Our study demonstrated that the levels of maximum radiodensity and skewness were independent risk factors for pathology. Furthermore, the combination of these two features significantly improved the

CT imaging signs	AAH / AIS (n = 80)	MIA (n = 59)	p
Shape			0.435
Round	50 (62.50%)	33 (55.93%)	
Non-circular	30 (37.50%)	26 (44.07%)	
Margins			0.536
Clear	27 (33.75%)	17 (28.81%)	
Blurred	53 (66.25%)	42 (71.19%)	
Spiculation			0.018
Present	20 (25.00%)	26 (44.07%)	
Absent	60 (75.00%)	33 (55.93%)	
Lobulation			0.086
Present	7 (8.75%)	11 (18.64%)	
Absent	73 (91.25%)	48 (81.36%)	
Vacuole sign			0.188
Present	19 (23.75%)	20 (33.90%)	
Absent	61 (76.25%)	39 (66.10%)	
Air bronchogram			0.081
Present	5 (6.26%)	9 (15.25%)	
Absent	75 (93.75%)	50 (84.75%)	
Pleural indentation			0.284
Present	3 (3.75%)	5 (8.47%)	
Absent	77 (96.25%)	54 (91.53%)	
Vascular convergence sign			0.525
Present	27 (33.75%)	23 (38.98%)	
Absent	53 (66.25%)	36 (61.02%)	
Pleural thickening			0.168
Present	9 (11.25%)	2 (3.39%)	
Absent	71 (88.75%)	57 (96.61%)	
Right lung	57 (71.25%)	37 (62.71%)	0.288
Upper lobe	31 (38.75%)	15 (25.42%)	0.082
Middle lobe	14 (17.50%)	5 (8.47%)	
Lower lobe	12 (15.00%)	17 (28.81%)	
Left lung	23 (28.75%)	22 (37.29%)	
Upper lobe	15 (18.75%)	12 (20.34%)	
Lower lobe	8 (10.00%)	10 (16.95%)	

**Table 2.** Semantic features of 139 cases of pGGOs diagnosed as MIA or precursor lesions. AAH, atypical adenomatous hyperplasia. AIS, adenocarcinoma in situ. MIA, minimally invasive adenocarcinoma. pGGO, pure ground-glass opacity.

diagnostic accuracy compared to using them individually. A pGGO with higher maximum radiodensity and smaller negative skewness is more likely to be MIA, possibly due to increased consolidation. This is consistent with previous studies<sup>36–38</sup>. However, it is important to note that CT features with significant differences did not demonstrate high diagnostic efficiency in our study, similar to previous research<sup>39</sup>. This suggests that further research utilizing radiomics and extracting more comprehensive imaging features from CT images is necessary to overcome the limitations of conventional imaging diagnosis and assist in classification and diagnosis.

According to multiple studies, both MIA and AIS have good prognosis. It has been shown 100% 5-year disease-free survival in both tumor types when completely resected<sup>10–15</sup>. However, during the process of AIS developing into MIA, there is an appearance of invasive component which is attributed to progression of invasiveness. Though the area of invasive component is quite small, as the same as it's in invasive adenocarcinoma, it could show different growth patterns in MIA, such as lepidic, acinar, papillary, micropapillary and solid pattern. Among these growth patterns, papillary pattern is found to be related to intermediate prognosis<sup>40</sup>. Whereas micropapillary and solid patterns are considered to be high-grade pattern because of their association of poor prognosis. It has been found that micropapillary growth is associated to lymphatic and pleural invasion and nodal metastases which are adverse prognostic factors<sup>13,29</sup>. Even a small amount of micropapillary pattern could lead to significantly worse overall survival<sup>41</sup>. In this case, if the invasive component in MIA appears high-grade growth pattern, it might not show the same prognosis as the common types do. There have been few studies that have investigated the prognosis of MIA with different invasive components. Jia et al. found a few cases of MIA showed papillary, micropapillary and solid pattern and all the cases showed recurrence or metachronous adenocarcinoma. Among these lesions, there is one that appears as pGGO showed papillary pattern<sup>16</sup>. Also, they



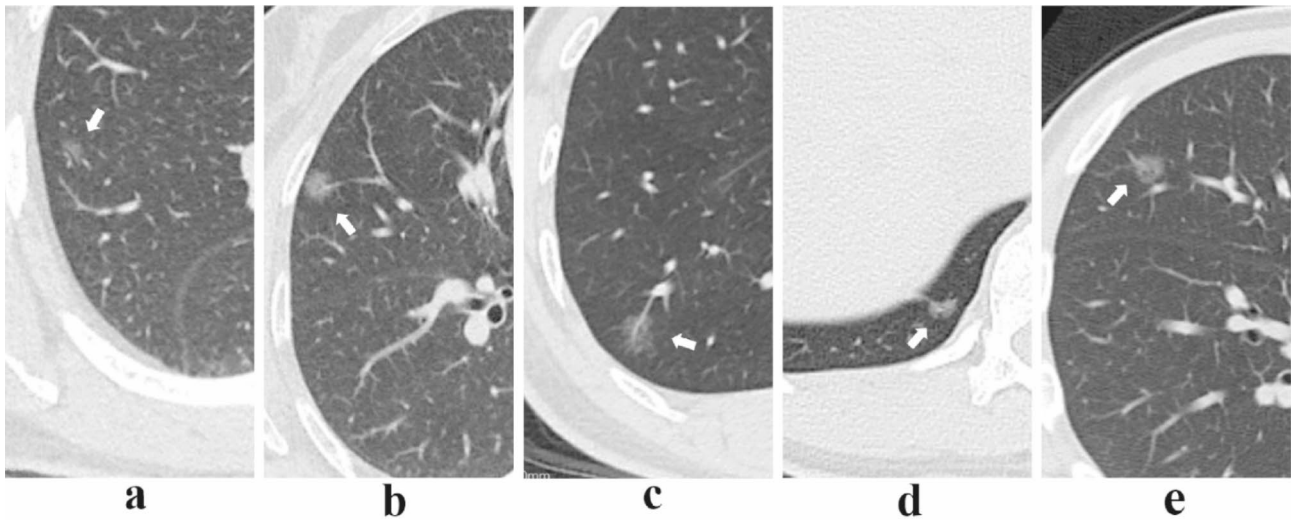


**Fig. 2.** CT images of pGGOs. (a) A 38-year-old male with an AIS lesion in the posterior segment of the right upper lobe, appearing as a non-circular and blurred-margin pGGO with air bronchogram. (b) A 63-year-old female with an AIS lesion in the outer segment of the right middle lobe, appearing as a round and blurred-margin pGGO with spiculation and vascular convergence sign. (c) A 44-year-old male with an MIA lesion in the outer basal segment of the right lower lobe, appearing as a non-circular and clear-margin pGGO with spiculation, lobulation and vascular convergence sign. (d) A 28-year-old female with an MIA lesion in the posterior basal segment of the right lower lobe, appearing as a non-circular and clear-margin pGGO with pleural indentation. (e) A 43-year-old male with an MIA lesion in the outer segment of the right middle lobe, appearing as a round and blurred-margin pGGO with spiculation, vacuole sign and vascular convergence sign. AIS, adenocarcinoma in situ. MIA, minimally invasive adenocarcinoma. pGGO, pure ground-glass opacity.

CT imaging quantitative parameters	AAH/AIS (n = 80)	MIA (n = 59)	p
Maximum diameter (mm)	8.00 (2.00)	8.00 (3.00)	0.776
3D maximum diameter (mm)	8.84 (3.58)	9.19 (3.25)	0.959
Maximum cross-sectional area (mm <sup>2</sup> )	42.44 (31.33)	44.69 (31.33)	0.873
Volume (mm <sup>3</sup> )	251.42 (336.29)	282.45 (321.77)	0.775
Maximum radiodensity (HU)	− 461.50 (219.00)	− 348.00 (234.00)	< 0.001
Minimum radiodensity (HU)	− 774.00 (141.00)	− 739.00 (212.00)	0.039
Mean radiodensity (HU)	− 629.49 (144.79)	− 530.64 (220.29)	< 0.001
Variance	79.45 (44.10)	93.64 (39.75)	0.005
Kurtosis	2.20 (0.32)	2.14 (0.20)	0.177
Skewness	− 0.17 (0.22)	− 0.19 (0.20)	0.035
Surface area (mm <sup>2</sup> )	221.16 (198.92)	248.19 (188.63)	0.611
Compactness	0.64 (0.27)	0.58 (0.24)	0.322
Sphericity	0.86 ± 0.08	0.85 ± 0.07	0.456
Entropy	8.54 ± 0.21	8.59 ± 0.17	0.190

**Table 3.** Shape features and first-order features of 139 cases of pGGO diagnosed as MIA or precursor lesions. Quantitative data with non-normal distribution was described by median (interquartile range) and quantitative data with normal distribution was described by mean ± standard deviation. AAH, atypical adenomatous hyperplasia. AIS, adenocarcinoma in situ. MIA, minimally invasive adenocarcinoma. pGGO, pure ground-glass opacity.

found significant differences in the expressions of p53, Ki67 and cyclin D1 and EGFR mutation rate between the AIS and MIA groups, which might associate with differences of tumor progression. In addition, Honda et al. found a pGGO containing micropapillary component and the same type of component was also found in mediastinal lymph nodes metastases<sup>42</sup>. Even though this lesion is invasive adenocarcinoma, this finding can still provide the prove of the possibility of existence of micropapillary component in pGGO and it's associated with lymph nodes metastases. Considering that the good prognosis of MIA being shown in other studies might be due to the low occurrence rate of these unique types of MIA, these factors that could affect prognosis should not be neglected when clinical decisions on MIA being made. Therefore, our findings in differences between

Features	Univariate analysis		Multivariate analysis	
	<i>p</i>	OR (95% CI)	<i>p</i>	OR (95% CI)
Maximum radiodensity (HU)				
< − 443.00	< 0.001		< 0.001	
− 443.00 to − 220.00	0.017	2.606 (1.188–5.718)	0.009	3.109 (1.330–7.266)
> − 220.00	< 0.001	13.054 (3.759–45.335)	< 0.001	12.955 (3.562–47.110)
Minimum radiodensity (HU)				
< − 775.00	0.006			
− 775.00 to − 660.00	0.176	1.725 (0.0.783–3.803)		
> − 660.00	0.001	4.706 (1.824–12.141)		
Mean radiodensity (HU)				
< − 650.00	< 0.001			
− 650.00 to − 564.00	0.244	1.785 (0.673–4.733)		
> − 564.00	< 0.001	5.355 (2.269–12.638)		
Variance				
< 80.50	0.002			
80.50 to 125.00	0.009	2.840 (1.305–6.180)		
> 125.00	0.002	6.345 (2.026–19.877)		
Skewness				
< − 0.07	0.011		0.045	
	0.004	0.111 (0.025–0.503)	0.013	0.136 (0.028–0.653)
> 0.02	0.233	0.500 (0.160–1.564)	0.806	0.858 (0.251–2.926)
Entropy				
< 8.45	0.016			
8.45 to 8.80	0.005	4.500 (1.565–12.940)		
> 8.80	0.361	2.200 (0.405–11.949)		

**Table 4.** Logistic regression model for differentiate MIA from precursor lesions. MIA, minimally invasive adenocarcinoma.

MIA and precursor lesions in pGGOs might have significant value on adjusting follow-up strategy or clinical treatment. The CT features with significant differences between MIA and precursor lesions could make a great help of improving the diagnostic accuracy of pathology and assisting precise management of patients.

This study has several limitations. Firstly, it is a single-center study, which may introduce selection bias and limit the generalizability of the results. Additionally, the relatively small number of cases in this study may have affected the accuracy of the statistical analysis and the clinical application of the research conclusions. Furthermore, the combination of the AAH and AIS groups in our study prevented us from exploring the differences in imaging features between AAH and the other two pathological subtypes. Also, all AAH lesions and most AIS/MIA lesions were resected due to their adjacency to other resected invasive adenocarcinomas, which might cause selection bias.

In conclusion, our study analyzed the correlation between CT imaging features of pGGOs and the pathological subtypes of AAH/AIS and MIA. We found significant differences in intensity features between the two groups, and maximum radiodensity and skewness were identified as independent risk factors for pathology. However, these features did not exhibit strong diagnostic efficiency. Future research should focus on utilizing radiomics and extracting more comprehensive imaging features to improve the accuracy of diagnosis and classification.

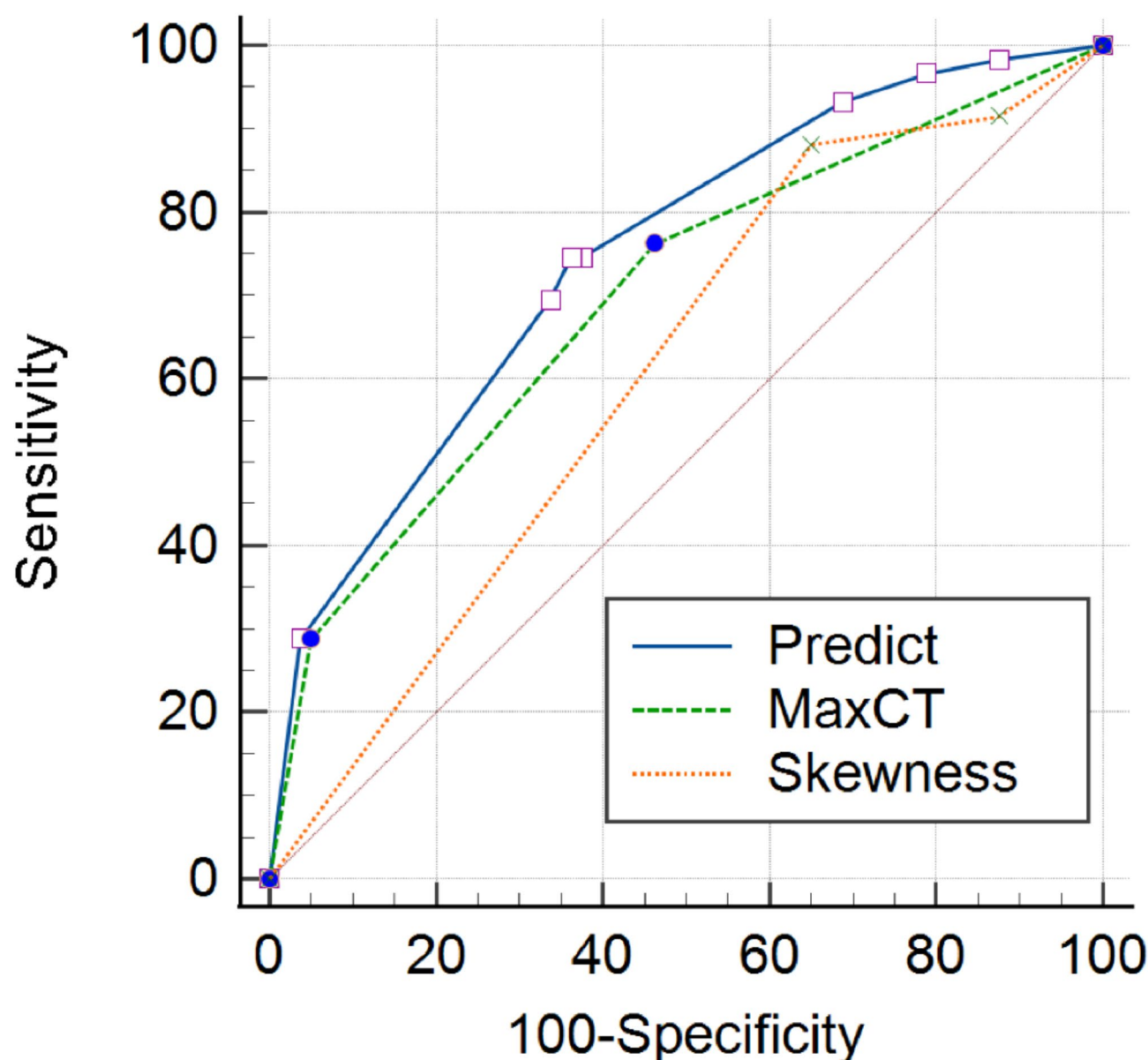


**Fig. 3.** The ROC curve of maximum radiodensity, skewness and predicted value of multivariate Logistic regression to distinguish AAH / AIS from MIA in pGGOs. AAH, atypical adenomatous hyperplasia. AIS, adenocarcinoma in situ. MIA, minimally invasive adenocarcinoma. pGGO, pure ground-glass opacity. ROC curve, receiver operating characteristic curve.

### Data availability

The data that support the findings of this study will be available from the corresponding author.

Received: 18 May 2024; Accepted: 24 February 2025

Published online: 04 March 2025

### References

1. Sung, H. et al. Global Cancer statistics 2020: GLOBOCAN estimates of incidence and mortality worldwide for 36 cancers in 185 countries. *CA Cancer J. Clin.* **1–41** (2021).
2. Zeng, H. et al. Changing cancer survival in China during 2003–15: A pooled analysis of 17 population-based cancer registries. *Lancet Glob. Health* **6**, e555–e567 (2018).
3. Toh, C. The changing epidemiology of lung cancer. *Methods Mol. Biol.* **472**, 397–411 (2009).
4. Zheng, R. et al. Analysis of the prevalence of malignant tumors in China in 2015. *Zhong Hua Zhong Liu Za Zhi* **41**, 19–28 (2019).
5. Kim, H. K. et al. Assessment of intratumoral heterogeneity of oncogenic driver mutations in surgically-resected lung adenocarcinoma: implications of percutaneous biopsy-based molecular assay for targeted therapy. *Anticancer Res.* **34**, 707–714 (2014).



6. Travis, W. D., Brambilla, E. & Riely, G. J. New pathologic classification of lung cancer: Relevance for clinical practice and clinical trials. *J. Clin. Oncol.* **31**(8), 992–1001 (2013).
7. Travis, W. D. et al. International association for the study of lung Cancer/american thoracic Society/european respiratory society international multidisciplinary classification of lung adenocarcinoma. *J. Thorac. Oncol.* **6**, 244–285 (2011).
8. Travis, W. D. et al. The 2015 world health organization classification of lung tumors: impact of genetic, clinical and radiologic advances since the 2004 classification. *J. Thorac. Oncol.* **10**, 1243–1260 (2015).
9. WHO Classification of Tumours Editorial Board. *Thoracic Tumours WHO Classification of Tumours* 5th edn, Vol. 5 (World Health Organization, 2021). Available at: <https://publications.iarc.fr/Book-And-Report-Series/Who-Classification-Of-Tumours/Thoracic-Tumours-2021>.
10. Wilshire, C. L. et al. Comparison of outcomes for patients with lepidic pulmonary adenocarcinoma defined by 2 staging systems: A North American experience. *J. Thorac. Cardiovasc. Surg.* **151**, 1561–1568 (2016).
11. Li, Y., Chen, Z., Yu, W. & Zhang, Y. Clinicopathology and prognosis of 489 patients with adenocarcinoma in situ and minimally invasive adenocarcinoma of lung. *Zhong Guo Xiong Xin Xue Guan Wai Ke Lin Chuang Za Zhi.* **24**, 445–449 (2017).
12. Gu, J. et al. Prognostic significance of the IASLC/ATS/ERS classification in Chinese patients-A single institution retrospective study of 292 lung adenocarcinoma. *J. Surg. Oncol.* **107**, 474–480 (2013).
13. Russell, P. A. et al. Does lung adenocarcinoma subtype predict patient survival? A clinicopathologic study based on the new international association for the study of lung Cancer/American thoracic society/European respiratory society international multidisciplinary lung adenocarcinoma classification. *J. Thorac. Oncol.* **6**, 1496–1504 (2011).
14. Tsuta, K. et al. The utility of the proposed IASLC/ATS/ERS lung adenocarcinoma subtypes for disease prognosis and correlation of driver gene alterations. *Lung Cancer* **81**, 371–376 (2013).
15. Yoshizawa, A. et al. Impact of proposed IASLC/ATS/ERS classification of lung adenocarcinoma: Prognostic subgroups and implications for further revision of staging based on analysis of 514 stage I cases. *Mod. Pathol.* **24**, 653–664 (2011).
16. Jia, M. et al. Clinicopathologic features and genetic alterations in adenocarcinoma in situ and minimally invasive adenocarcinoma of the lung: Long-term follow-up study of 121 Asian patients. *Ann. Surg. Oncol.* **27**(8), 3052–3063 (2020).
17. Zhao, Y. & Yu, J. Review of radiomics in lung adenocarcinoma manifesting as ground glass nodule. *Zhong Guo Yi Liao She Bei.* **36**, 167–171 (2021).
18. Zhu, X. et al. The value of CT in the early diagnosis of ground-glass pulmonary nodules. *Zhong Guo Lin Chuang Yi Sheng Za Zhi.* **46**, 435–437 (2018).
19. National Lung Screening Trial Research Team. Results of initial low-dose computed tomographic screening for lung cancer. *N. Engl. J. Med.* **368**, 1980–1991 (2013).
20. Si, M. J. et al. Thin-section computed tomography-histopathologic comparisons of pulmonary focal interstitial fibrosis, atypical adenomatous hyperplasia, adenocarcinoma in situ, and minimally invasive adenocarcinoma with pure ground-glass opacity. *Eur. J. Radiol.* **85**, 1708–1715 (2016).
21. Hansell, D. M. et al. Fleischner society: Glossary of terms for thoracic imaging. *Radiology* **246**, 697–722 (2008).
22. Wang, Z. & Xu, G. The radiology, pathology and clinical management of grand-glass opacity lung nodules. *Xian Dai Zhong Liu Yi Xue.* **26**, 793–796 (2018).
23. Qi, L. et al. Analysis of CT morphologic features and Attenuation for diferentiating among transient lesions, atypical adenomatous hyperplasia, adenocarcinoma in situ, minimally invasive and invasive adenocarcinoma presenting as pure ground-glass nodules. *Sci. Rep.* **9**, 14586 (2019).
24. Chu, Z. G., Li, W. J., Fu, B. J. & Lv, F. J. CT characteristics for predicting invasiveness in pulmonary pure ground-glass nodules. *AJR Am. J. Roentgenol.* **215**, 351–358 (2020).
25. Wang, L. et al. Nomogram for predicting the risk of invasive pulmonary adenocarcinoma for pure ground-glass nodules. *Ann. Thorac. Surg.* **105**, 1058–1064 (2018).
26. Zhang, Y. et al. Results of low-dose computed tomography as a regular health examination among Chinese hospital employees. *J. Thorac. Cardiovasc. Surg.* **160**, 824–831 (2020).
27. Li, X. et al. The epidemiology of ground glass opacity lung adenocarcinoma: A network-based cumulative meta-analysis. *Front. Oncol.* **10**, 1059 (2020).
28. Lin, H. T. et al. Epidemiology and survival outcomes of lung cancer a population-based study. *BioMed. Research. Int.* 1–19 (2019).
29. Yoshizawa, A. et al. Validation of the IASLC/ATS/ERS lungadenocarcinoma classification for prognosis and association with EGFR and KRAS gene mutations: Analysis of 440 Japanese patients. *J. Thorac. Oncol.* **8**, 52–61 (2013).
30. Liu, S. et al. Precise diagnosis of intraoperative frozen section is an effective method to guide resection strategy for peripheral Small-Sized lung adenocarcinoma. *J. Clin. Oncol.* **34**, 307–313 (2016).
31. Altorki, N. K. et al. Sublobar resection is equivalent to lobectomy for clinical stage 1A lung cancer in solid nodules. *J. Thorac. Cardiovasc. Surg.* **147**, 754–762 (2014).
32. Wang, S., Fu, Z. & Qiu, J. Progress in the diagnosis of lung adenocarcinoma manifesting as ground glass nodule. *Guo Ji Yi Xue Fang She Xue Za Zhi* **44**, 67–71 (2021).
33. Hara, M. et al. Focal fibrosis as a cause of localized ground glass Attenuation (GGA)—CT and MR findings. *Radiat. Med.* **20**, 93–95 (2002).
34. Zhan, Y. et al. Attenuation and morphologic characteristics distinguishing a Ground-Glass nodule measuring 5–10 mm in diameter as invasive lung adenocarcinoma on Thin-Slice CT. *AJR Am. J. Roentgenol.* **213**, W162–W170 (2019).
35. Qi, L. et al. Analysis of CT morphologic features and Attenuation for differentiating among transient lesions, atypical adenomatous hyperplasia, adenocarcinoma in situ, minimally invasive and invasive adenocarcinoma presenting as pure ground-glass nodules. *Sci. Rep.* **9**, 14586 (2019).
36. Zhang, T. et al. Histogram analysis combined with morphological characteristics to discriminate adenocarcinoma in situ or minimally invasive adenocarcinoma from invasive adenocarcinoma appearing as pure ground-glass nodule. *Eur. J. Radiol.* **113**, 238–244 (2019).
37. Wang, X. et al. Can we differentiate minimally invasive adenocarcinoma and non-invasive neoplasms based on high-resolution computed tomography features of pure ground glass nodules? *PLoS One* **12**, e0180502 (2017).
38. Kamiya, A. et al. Kurtosis and skewness assessments of solid lung nodule density histograms: Differentiating malignant from benign nodules on CT. *Jpn. J. Radiol.* **32**, 14–21 (2014).
39. Xiang, W. et al. Morphological factors differentiating between early lung adenocarcinomas appearing as pure ground-glass nodules measuring  $\leq 10$  mm on thin-section computed tomography. *Cancer Imaging.* **14**, 33 (2014).
40. Warth, A. et al. The novel histologic international association for the study of lung Cancer/American thoracic society/European respiratory society classification system of lung adenocarcinoma is a stage-independent predictor of survival. *J. Clin. Oncol.* **30**, 1438–1446 (2012).
41. Lee, G. et al. Clinical impact of minimal micropapillary pattern in invasive lung adenocarcinoma: Prognostic significance and survival outcomes. *Am. J. Surg. Pathol.* **39**, 660–666 (2015).
42. Honda, Y. et al. Mediastinal lymph node metastases in lung cancer presenting as pure ground-glass nodules: A surgical case report. *Int. J. Surg. Case Rep.* **70**, 5–7 (2020).

## Author contributions

All authors contributed to the study conception and design. Y.Z., Y.C., W.T., Y.D. and C.B. performed data collection. Y.Z., Y.D., W.T., X.C. and Y.G. reviewed the images. Y.Z., Y.C., Y.D. and W.L. performed data analysis. All authors contributed to interpretation of the data. The first draft of the manuscript was written by Y.Z., all authors helped revised the manuscript. All authors read and approved the final manuscript.

## Funding

This study has received funding by the National Natural Science Foundation of China Special Program for Cultivation of the Third Affiliated Hospital of Sun Yat-sen University [grant number 2021GZRPYMS06]; Five-five Project of the Third Affiliated Hospital of Sun Yat-sen University [grant number 2023WW605].

## Declarations

## Competing interests

The authors declare no competing interests.

## Additional information

**Supplementary Information** The online version contains supplementary material available at <https://doi.org/10.1038/s41598-025-91902-3>.

**Correspondence** and requests for materials should be addressed to J.Q.

**Reprints and permissions information** is available at [www.nature.com/reprints](http://www.nature.com/reprints).

**Publisher's note** Springer Nature remains neutral with regard to jurisdictional claims in published maps and institutional affiliations.

**Open Access** This article is licensed under a Creative Commons Attribution-NonCommercial-NoDerivatives 4.0 International License, which permits any non-commercial use, sharing, distribution and reproduction in any medium or format, as long as you give appropriate credit to the original author(s) and the source, provide a link to the Creative Commons licence, and indicate if you modified the licensed material. You do not have permission under this licence to share adapted material derived from this article or parts of it. The images or other third party material in this article are included in the article's Creative Commons licence, unless indicated otherwise in a credit line to the material. If material is not included in the article's Creative Commons licence and your intended use is not permitted by statutory regulation or exceeds the permitted use, you will need to obtain permission directly from the copyright holder. To view a copy of this licence, visit <http://creativecommons.org/licenses/by-nc-nd/4.0/>.

© The Author(s) 2025